Bioresource Technology Reports 22 (2023) 101500

Contents lists available at ScienceDirect

Bioresource Technology Reports

journal homepage: www.sciencedirect.com/journal/bioresource-technology-reports

Thermogravimetric kinetic-based computation of raw and pretreated coconut husk powder lignocellulosic composition

Akbarningrum Fatmawati, Tantular Nurtono, Arief Widjaja *

Chemical Engineering Department, Institut Teknologi Sepuluh Nopember, Kampus ITS Sukolilo, Surabaya 60111, Indonesia

ARTICLE INFO

Keywords:
Coconut husk
Pyrolysis kinetic
Thermogravimetry
Biomass
Activation energy

ABSTRACT

Lignocellulosic biomass is one of the potential sources for biofuel production. Coconut husk, one of the abundant lignocellulosic biomass in Indonesia, can be explored for such a process. This work evaluated compositions of raw and pretreated coconut husk powder using modeling and computation of thermogravimetry analysis data. Lignocellulose compositions and distributed activation energy model employing kinetic parameters were successfully obtained with the fit quality values of 0.1–0.35 %, and R-squared values (R^2) equal 1. By this method, raw coconut husk powder was found to contain 30 % hemicellulose, 38.86 % cellulose, and 34.96 % lignin. The mean activation energy (E_0) was 141–163, 173–181, and 200–230 kJ/mol for hemicellulose, cellulose, and lignin respectively. Meanwhile, the standard deviation activation energy (σ) was 4.8–7.5, 1.76–3.75, and 19–28 kJ/mol for hemicellulose, cellulose, and lignin respectively. The pre-exponential factor (A) values ranged from 1.20×10^{11} to 5.00×10^{13} s^{-1} where those of hemicellulose, cellulose, and lignin, respectively appeared in ascending order.

1. Introduction

The recent issues of rapid fossil fuel reserves depletion and climate change, which is apparently caused by CO_2 emission, have driven new policies development on bio-based clean energy usage and consequently propelled scientific works exploring lignocellulosic biomass (LCB) to produce alternative fuels and chemicals (Sydney et al., 2019). In 2021 the global CO_2 emission had increased by 6 % from 2020 when the pandemic Covid 19 had caused the largest-ever emission decline albeit it still reached the value of 31.5 Gt and the highest-ever average annual concentration of 412.5 ppm in the atmosphere. This concentration was 50 % higher than that in the beginning era of the industrial revolution (IEA, 2021). According to Raud et al. (2019) the temperature increase had evidently reached 0.85 °C compared to the preindustrial era and resulted in sea level rise as well as other climate change facts. Bioenergy, renewable energy sources produced from biomass, is expected to play a key role in the attempt to manage the Net Zero Emission scenario by 2050. Between 2010 and 2021, its average use increased to 7 % per year, and this is expected to increase by 2030 in several applications such as biojet kerosene, liquid biofuel, industry, and electricity generation (Hodgson et al., 2022). Supporting the fact of LCB conversion to bioenergy need, the global LCB production yield had been reported enormous as it reached 1.3 billion tons per year (Baruah et al., 2018). Coconut husk is one of the enormous agricultural food wastes in Indonesia as the largest producer of the coconut fruit. Therefore, it can be a potential lignocellulose material for alternative fuel and chemical production.

Biomass to biofuel and biochemical conversion can be accomplished through thermochemical or biochemical route, by which several types of biofuels such as gaseous fuel (methane and hydrogen), pyrolysis oil, and bioethanol can be produced (Menon and Rao, 2012). Despite LCB's great potential for alternative fuel and chemical sources, its utilization still hands over obstacles concerning recalcitrant properties upon biochemical conversion caused by its hardly hydrolytic enzyme accessed structural components (hemicellulose, cellulose, and lignin) characteristic. Many pretreatment methods prior to enzymatic hydrolysis had been applied to LCB to enhance the rate of enzymatic hydrolysis reaction which is inhibited by the presence of lignin as well as the crystalline characteristic of cellulose molecule (Menon and Rao, 2012; Raud et al., 2019). Pretreatment using ultrasound at low frequency (20–80 kHz) offers a quite promising method to change the surface area and structure of lignocellulose biomass which can become more amenable to hydrolytic enzyme attack. The violent cavitation brought about by low-frequency ultrasound leads to physical effects such as microjet impact

* Corresponding author.
E-mail address: arief_w@chem-eng.its.ac.id (A. Widjaja).

https://doi.org/10.1016/j.biteb.2023.101500
Received 26 January 2023; Received in revised form 4 June 2023; Accepted 7 June 2023
Available online 9 June 2023

and shockwave damage on the solid surface (Kuna et al., 2017). Meanwhile, the physicochemical process employing subcritical water or liquid hot water also renders a promising process of lignocellulose biomass conditioning. Subcritical water, which exists between its normal boiling point (100 °C) and critical point (374 °C and 22.1 MPa) with adjusted pressure to maintain liquid phase has drastic changes in its properties such as the increase in the ionic product (kw), drop in dielectric constant and density decrease. These changes favor the chemical transformation of the lignocellulose material being treated. Incorporating gas CO_2 into the subcritical water can boost the expected reaction in the subcritical water pretreatment of lignocellulose biomass (Prado et al., 2016; Ruiz et al., 2013).

Generally, the design and economic feasibility analysis of a chemical process plant requires the calculation of mass and energy balance and process yield. Similarly, the design of LCB to biofuel conversion also requires such calculations which demand compositional analysis of both solid and liquid fractions (Templeton et al., 2016). The lignocellulose compositional analysis of the solid fraction usually uses a suite of summative methods consisting of two-step sulfuric acid hydrolysis followed by HPLC analysis of sugar components. The method had been continuously developed by various process temperature and time changes to obtain the best condition approaching 100 % total closure. Such a method was also promulgated by a standard organization such as the Technical Association of the Pulp and Paper Industry (TAPPI). It was National Renewable Energy Laboratory (NREL) that applied the method to biofuel feedstock and disseminated it through the American Society for Testing and Materials (ASTM) to increase its industrial relevance (Sluiter et al., 2010). The current suite used by NREL consists of 72%w sulfuric acid treatment of extractive-free biomass at 30 °C for 1 h followed by dilution into 4%w sulfuric acid concentration and boiling at 121 °C for 1 h. The solid fraction from this sulfuric acid treatment represents the acid-insoluble lignin while the liquid fraction, having been neutralized, can be analyzed for monomeric sugar composing the carbohydrate using HPLC (Sluiter et al., 2012). The other even more conventional and widely used gravimetric method, the Chesson-Datta method, comprises a series of three-step sulfuric acid destruction with filtration plus washing, drying, and solid mass measurement in between to obtain the composition of hemicellulose, cellulose, and lignin following extraction. The first destruction boils the solid sample in 0.5 M (±4.74 %) sulfuric acid for 2 h while the second destruction employs soaking the solid in 72%v/v sulfuric acid solution followed by diluting to 0.5 M and boiling (Cheng et al., 2019; Nurika et al., 2022). These reveal that both gravimetry and summative method suites are time-consuming and use hazardous treatment solutions. Moreover, incomplete acid destruction may bias the composition result.

Thermogravimetric analysis (TGA) is a thermo-analytical technique for solid-phase material degradation studies. Using a TGA analyzer, one can obtain information on mass changes as a function of temperature and time under a controlled atmosphere (Emiola-Sadiq et al., 2021; Xiang et al., 2022). This technique is potential to be exploited for lignocellulose composition determination to replace the tedious gravimetric method (Cai et al., 2017). As mass changes are detectable and recordable while pyrolysis reaction occurs in this analysis, employing appropriate kinetic models which incorporate LCB components and computation methods will allow faster LCB composition determination. Several attempts to utilize TGA data for LCB compositional analysis have existed (Cai et al., 2013; Chen et al., 2015; Kim et al., 2022; Lopes and Tannous, 2020; Rego et al., 2019). According to Hu et al., 2016, the three-parallel-reaction (TPR) model is the most suitable multi-step reaction model for representing lignocellulose biomass pyrolysis kinetic, and there are three calculation procedures corresponding to this model which are order-based mechanism, distributed activation energy model (DAEM), and deconvolution. Cai et al., 2013 applied DAEM to obtain the thermogravimetry (TG) kinetic parameters of xylan and cellulose and fitted the three-parallel DAEM-reaction model to the derivative thermogravimetry (DTG) data of 8 different LCBs. This fitting resulted in lignocellulose compositions in spite of kinetic parameters. Other works fitted the DTG data without incorporating DAEM to obtain lignocellulose composition (Kim et al., 2022; Lopes and Tannous, 2020). Rego et al. (2019) applied the deconvolution method using the Gaussian peak function to evaluate the lignocellulosic composition of Poplar. Hu et al. (2016) applied DAEM in DTG fitting and also attempted to employ the Fraser-Susuki deconvolution procedure. Chen et al. (2015) applied the DAEM to another 5 LCB materials but used experimental TG data for fitting as this was more accurate than DTG data.

In this work, compositions of raw as well as ultrasonic and subcritical water pretreated coconut husk powder (CHP) were determined from thermogravimetric analysis data. The method employed a three-parallel-reaction model which incorporated distributed activation energy model (DAEM) in TG data fitting. To the best of authors' knowledge, this attempt has not been applied to raw, ultrasonic, and subcritical water pretreated coconut husk. The assumption used in developing this model was the existence of reactions with a range of activation energies during the decomposition of complex biomass. The Gaussian distribution function was used to characterize the activation energy distribution.

2. Materials and methods

2.1. Materials

Coconut husk, the mesocarp of the coconut fruit, was acquired from local market waste. The mesocarp was washed and dried under sunlight. The dry mesocarp was then cut and ground using a disc mill machine. The CHP with the size range of 0.21–0.40 mm, studied in this work, was collected after screening the ground coconut husk. Pure-grade sulfuric acid (98 %, PT. Smart-Lab, Indonesia) was used as a medium in the ultrasonic pretreatment. Sodium dodecyl sulfate (Reagent Plus® >98.5 %, Sigma Aldrich, Germany) was used in the subcritical water pretreatment. Gas CO_2 (99 %, Samator Co., Indonesia) was used in the subcritical water pretreatment and Gas N_2 (99.999 %, Samator Co., Indonesia) was used in TGA.

Proximate and ultimate analysis was conducted to obtain the characteristic of the husk. The analyses were performed according to ASTM protocol at the certified analysis laboratory of Sucofindo Co. The proximate analysis comprised total moisture, ash, volatile matter, fixed carbon, total sulfur, and gross caloric value. The total moisture was determined using an oven-drying method (ASTM E871-82). The ash content was performed by weight measurement of solid residue after in-furnace heating of one gram sample at 500 °C for 1 h followed by heating to 750 °C for 2 h (ASTM D3174-12). The volatile matter (ASTM D3175-20) corresponded to the weight loss after heating one gram sample at 950 °C for 7 min. The fixed carbon (D3172-13) was the resultant of the moisture, ash, and volatile matter summation subtracted from 100. The total sulfur content was determined by sample combustion at 1350 °C to oxidize sulfur (ASTM D4239-18). The gross caloric value was obtained after carrying out sample combustion in a calorimeter (ASTMD5865-19). The ultimate analysis, which included the carbon, hydrogen, and nitrogen content was performed according to ASTM D5373-21 standard. The oxygen content was obtained by subtracting the sum of C, H, and N content in percentage from 100 (ASTM D3176-15).

2.2. Pretreatment

The ultrasonic pretreatment was conducted using an ultrasonic bath (Elma LC 20H, Germany) with a frequency of 35 kHz and power of 100 W. The equipment was modified by attaching a thermocouple and its controller (Autonics TC4S). The CHP slurry was made by mixing CHP and distilled water with a solid-to-liquid ratio of 1:20.

The subcritical water pretreatment used a stainless-steel cylindrical reactor with a total volume of 420 mL and a working volume of about 150 mL. The reactor was equipped with an electrical heating jacket,

temperature controller (Autonics TZN4S), and pressure gauge. Gas CO_2 was supplied to the reactor to attain an initial pressure of 60 bar.

2.3. Thermogravimetric analysis

Thermogravimetry analysis (TGA) was done using a thermogravimetric analyzer (TGA/DSC1, Mettler Toledo, Columbus, Switzerland) run at linear temperature program with 10 °C/min heating rate. The atmospheric gas used was N_2 with the rate of 50 mL min^{-1}. The sample amounts were 6 mg for raw CHP and 2.8–3.0 mg for treated CHP. The samples were placed in a 40 μL aluminum crucible and heated from 25 to 600 °C.

2.4. Kinetic modeling

2.4.1. Pyrolysis reaction kinetics

The global reaction kinetic model representing the solid-state pyrolysis reaction in TGA has been elaborated in several works (Dash et al., 2022; Van Geem, 2019). The rate is commonly expressed using conversion instead of concentration (Vyazovkin, 2016). The rate temperature dependence is described using the Arrhenius equation as shown in Eq. (1):

$$r = \frac{d\alpha}{dt} = k(T).f(\alpha) = Aexp\left(-\frac{E}{RT}\right).f(\alpha) \tag{1}$$

where r is the reaction rate (K^{-1}), α is the reaction conversion, $f(\alpha)$ is a conversion dependence function, A is pre-exponential factor (s^{-1}), E is apparent activation energy (J mol^{-1}), and R is the ideal gas constant (8.3145 J mol^{-1} K^{-1}). The temperature dependence of the reaction conversion can be derived based on the relationship shown in Eq. (2):

$$\frac{d\alpha}{dT} = \frac{d\alpha}{dT} \times \frac{dt}{dT} = \frac{d\alpha}{dT} \times \frac{1}{\beta} \tag{2}$$

where β is the constant heating rate (K min^{-1}) and T is the absolute temperature (K). The kinetic equation is then expressed as in Eq. (3):

$$r = \frac{d\alpha}{dT} = \frac{A}{\beta} exp\left(-\frac{E}{RT}\right) f(\alpha) \tag{3}$$

The independent variable conversion (α) is defined as:

$$\alpha = \frac{m_0 - m_t}{m_0 - m_f} \tag{4}$$

where m_0, m_t and m_f are the initial, instant, and final mass of the samples.

The Integration of Eq. (3) results in the following equation:

$$g(\alpha) = \int_0^\alpha \frac{1}{f(\alpha)} d\alpha = \frac{A}{\beta} \int_{T0}^{T} exp\left(-\frac{E}{RT}\right) dT = \frac{A}{\beta} \psi(E,T) \tag{5}$$

where $g(\alpha)$ is the integral of $1/f(\alpha)$, and $\psi(E,T)$ is the integral of exponential of minus E/RT. This integral has no analytical solution but it can be solved using Senum & Yang 4th-degree rational approximation (Aghili, 2021; Deng et al., 2009):

$$\psi(E,T) \approx \int_{T0}^{T} exp\left(-\frac{E}{RT}\right) dT = \frac{E}{R} \frac{exp(-x)}{x} \pi(x) \tag{6}$$

where x = E/RT and

$$\pi(x) = \frac{x^3 + 18x^2 + 86x + 96}{x^4 + 20x^3 + 120x^2 + 240x + 120} \tag{7}$$

Using first-order reaction assumption, where $f(\alpha) = 1\text{-}\alpha$, the integral in the left term of Eq. (5) can be solved and result in the following expression:

$$1 - \alpha = exp\left[-\frac{A}{\beta}\psi(E,T)\right] \tag{8}$$

The expression shown in Eq. (8) was then used in this work to evaluate the CHP devolatilization conversion in each stage as described in Subsection 2.4.2.

2.4.2. Pyrolysis stages identification from mass loss data

Three pyrolysis stages can be observed through the TG, first derivative thermogravimetric (DTG), and second derivative thermogravimetric (DDTG) curves. From the TGA data, a mass loss profile can be constructed using a plot of the remaining mass of volatile versus temperature. The normalized remaining volatile mass was calculated according to Eq. (9):

$$Y = \frac{m_t - m_f}{m_0 - m_f} \tag{9}$$

where Y = normalized remaining mass of volatiles. The DTG and DDTG data were calculated from normalized remaining mass, as follows:

$$Y'_T = \frac{Y_{T+\Delta T} - Y_T}{\Delta T} \tag{10}$$

$$Y''_T = \frac{Y'_{T+\Delta T} - Y'_T}{\Delta T} \tag{11}$$

where Y'_T, and Y''_T = first, and second derivative of Y.

2.4.3. Three-parallel DAEM and stage conversion modeling

In the distributed activated energy model (DAEM), numerous first-order independent decomposition reactions of organic material occur. The model assumes the same pre-exponential factor (A) for those reactions and adopts the Gaussian probability distribution function for the activation energy (Hu et al., 2016; Chen et al., 2015). The continuous distribution of activation energy is expressed in Eq. (12):

$$f(E) = \frac{1}{\sigma\sqrt{2\pi}} exp\left[-\frac{(E - E_0)^2}{2\sigma^2}\right] \tag{12}$$

where E_0 is the mean and σ is standard deviation of activation energy. The temperature-dependence function of conversion therefore can be expressed as follows:

$$1 - \alpha = \int_0^\infty exp\left(-\frac{A}{\beta}\psi(E,T)\right) f(E) dE \tag{13}$$

Following the stage division, the pyrolysis reaction kinetic parameters in every stage can be evaluated by combining Eqs. (12) and (13), as follows:

$$\alpha_i = 1 - \int_0^\infty exp\left(-\frac{A_i}{\beta}\psi(E,T)\right) \frac{1}{\sigma_i\sqrt{2\pi}} exp\left[-\frac{(E - E_{0i})^2}{2\sigma_i^2}\right] dE \tag{14}$$

For each of the stages, the values of A_i, $E_{0,i}$, and σ_i were determined numerically such that the following least square objective function is minimized:

$$F_1 = \sum_{j=1}^{N_{d,i}} \left(\alpha_{j,exp} - \alpha_{j,calc}\right)^2 \tag{15}$$

where $\alpha_{j,exp}$ and $\alpha_{j,calc}$ are the conversions obtained from experiments and model calculation, respectively while $N_{d,i}$ is the number of data of the i-th stage.

2.4.4. Mass loss modeling

The instantaneous mass loss for each of infinite volatile substances involved in the first-order reactions based on DAEM was modeled by

Table 1
Coconut husk powder characteristic.

Properties	This work		Other work***
	AR*	DB**	DB
Proximate (%wt):			
Moisture	8.09	–	–
Volatile matter	64.06	69.90	79.61 ± 2.09
Fixed carbon	24.10	26.23	17.50 ± 2.43
Ash	3.75	4.08	2.90 ± 0.36
Total sulfur	0.07	0.07	0.19 ± 0.07
Caloric value (MJ/kg)	18.1837	19.7819	17.70 ± 0.07
Ultimate (%wt):			
C	46.68	50.79	46.54 ± 0.21
H	4.55	4.95	6.88 ± 0.29
O	36.73	39.97	43.13 ± 0.01
N	0.13	0.14	0.36 ± 0.02

Notes: *AR = as received; **DB = dry basis; *** Lopes and Tannous (2020).

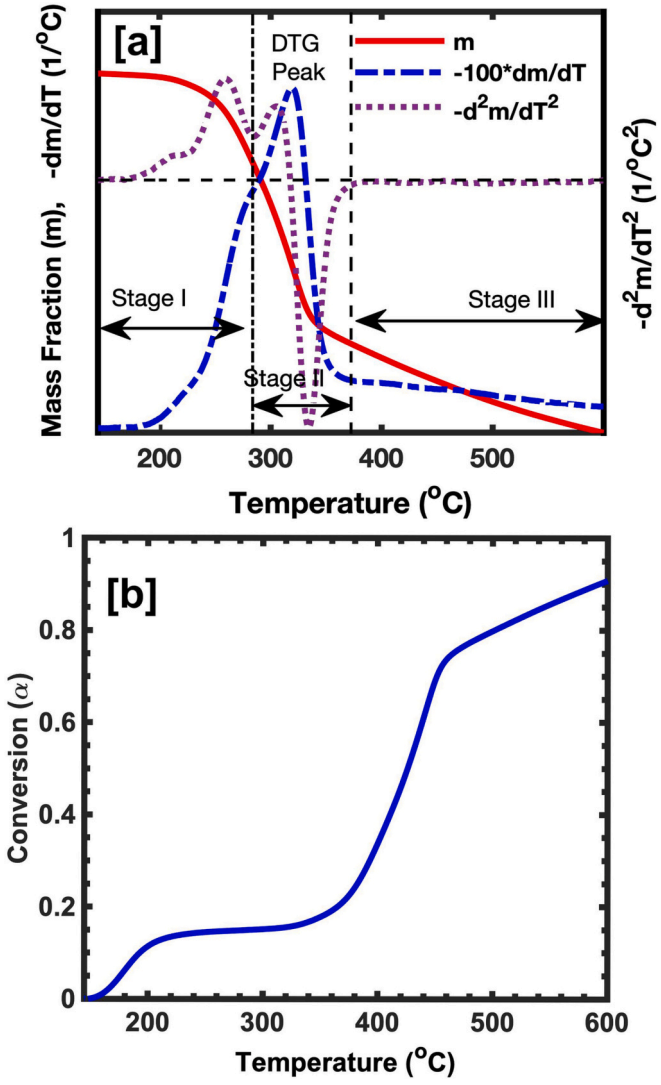

Fig. 1. (a) TGA, DTG, and DDTG profile with the pyrolysis stage division; (b) total conversion profile of volatile substances.

(Chen et al., 2015) as follows:

$$-\frac{dM_{p,i}}{dT} = \frac{A_{p,i}}{\beta} exp\left(-\frac{E_{p,i}}{RT}\right) M_{p,i} \tag{16}$$

where $M_{p,i}$ is the instantaneous mass of the volatile substance number p of the i-th pseudo-component. There are 3 pseudo-components composing the lignocellulosic biomass. Hence, each of the pseudo-components (hemicellulose, cellulose, lignin) fractional mass which comprises a large number of volatile substances was evaluated using the following expressions:

$$m_i = \int_0^{\infty} M_{p,i} dE \tag{17}$$

and

$$m_{i,0} = \int_0^{\infty} M_{p,i,0} dE \tag{18}$$

where m_i is pseudo-component fractional mass at a certain time or temperature and $m_{i,0}$ is initial pseudo-component fractional mass. As the lignocellulose biomass produces volatile substances and char upon decomposing, the total mass of the biomass can be formulated as in Eq. (19):

$$m = \sum_{i=1}^{3} m_i + m_c \tag{19}$$

The expression of the lignocellulose biomass mass change function is as follows:

$$m = m_c + \sum_{i=1}^{3} c_i (1 - m_c) \int_0^{\infty} exp\left(-\frac{A_i}{\beta} \psi(E,T)\right) \frac{1}{\sigma_i \sqrt{2\pi}} exp\left[-\frac{(E - E_{0i})^2}{2\sigma_i^2}\right] dE \tag{20}$$

where c_i (i = 1,2, and 3) represents the composition of hemicellulose, cellulose,and lignin, respectively. The values of 11 parameters (A_1, A_2, A_3, $E_{0,1}$, $E_{0,2}$, $E_{0,3}$, α_1, α_2, α_3, c_1, c_2) in Eq. (20) were obtained by minimizing the following least square objective function:

$$F_2 = \sum_{j=1}^{N_d} \left(m_{j,exp} - m_{j,calc}\right)^2 \tag{21}$$

where $m_{j,exp}$, and $m_{j,calc}$ are the mass fraction obtained from experiments and model calculation, respectively while N_d is the number of data.

2.4.5. Computation aid and optimization evaluation

The TGA data, and the calculation of values of Y, and were performed and stored using Microsoft Excel®. The stored data were called in MATLAB® m-file for further calculations including Y, Y'_T, and Y''_T. As derivation using such discrete data resulted in a noisy curve, a twice-smoothing procedure was performed for each of the derivations. The first smoothing used spline function while the second one used mov-mean function of MATLAB®.

The minimization calculations of objective functions to obtain the kinetic parameters, as well as lignocellulosic composition, were carried out using MATLAB® (version R2021b) software. The minimization used *lsqnonlin* function with the Levenberg-Marquardt algorithm. The software also provided the built-in *integral* function needed in this work.

The coefficient of determination (R^2) was calculated to describe the quality of optimization result using the following equation:

$$R^2 = 1 - \frac{SSE}{SST} \tag{22}$$

where SSE = sum of squared residuals and SST = total sum of squares, representing the total amount of fit variations. The SSE values were the same as objective function (F_1 for fitting the stage conversion, or F_2 for

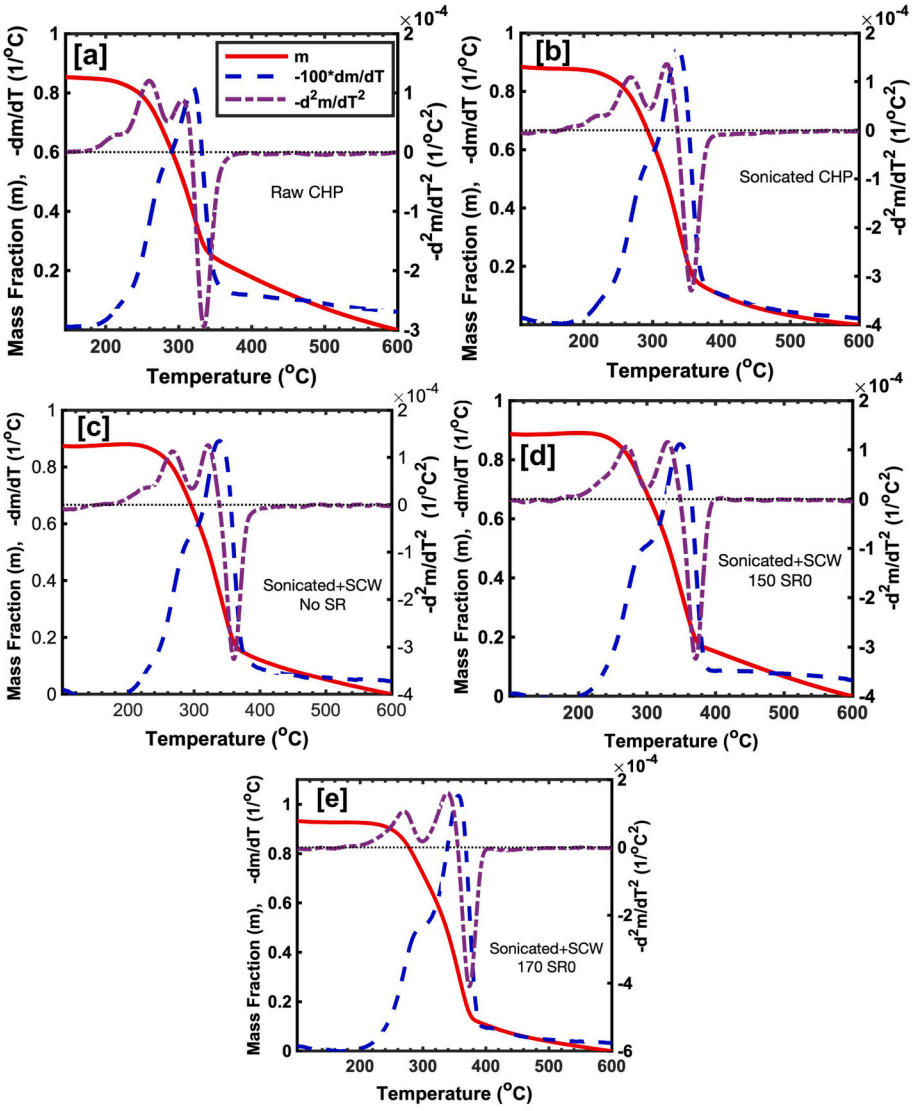

Fig. 2. The TG, DTG, and DDTG profile. (a) Raw CHP, (b) sonicated CHP using water medium at 60 °C for 30 min, and sonicated and SCW treated at (c) 150 °C for 60 min without surfactant addition, (d) 150 °C for 60 min with 2 % surfactant addition, and (e) 170 °C for 80 min with 2 % surfactant addition.

Table 2
Pyrolysis stage and peak temperature.

Sample	Initial temperature (T_i), °C			T_{peak}, °C	CI, %
	Stage I	Stage II	Stage III		
Raw CHP	150	285.00	368.83	319	69.4416
Sonicated CHP	150	296.00	390.67	336	70.3193
150/60/NSR	150	296.33	387.33	338	82.7632
150/60/SR2%	150	298.83	403.00	349	74.0484
170/80/SR2%	150	299.33	401.33	357	72.1946

Notes: T_i = initial temperature; CI = Crystallinity index.

fitting the pseudo component composition) while *SST* can be calculated as follows:

$$SST = \sum_{i=1}^{n} \left(\alpha_{i,exp} - \overline{\alpha_{exp}}\right)^2 \quad (23)$$

for fitting the stage conversion, or

$$SST = \sum_{i=1}^{n} \left(m_{exp} - \overline{m_{exp}}\right)^2 \quad (24)$$

for mass loss fitting, where $\overline{\alpha_{exp}}$ is the average experimental stage conversion, and $\overline{m_{exp}}$ is the average experimental normalized mass. Fit quality was used to assess the fitting results to obtain the model parameters following the expression below:

$$FQ(\%) = \frac{100 \times \sqrt{\frac{F}{N_d - N_p - 1}}}{h} \quad (25)$$

where $F = F_1$ or F_2, N_p = number of parameters in equation Eqs. (14) and (20), and h = maximum amount of α_{exp} in Eq. (23) or m_{exp} in Eq. (21). This fit quality equation is the standard deviation percentage.

2.5. Crystallinity index determination

The sample crystallinity index (CI) was evaluated using the X-Ray Diffraction (XRD) spectra data. The instrument, X'Pert PRO (PANalytical BV, Netherland), was operated using Cu Kα radiation with 40 kV and 30 mA electric current. Based on the empirical Segal method (Cheng et al., 2019; Ling et al., 2017) the following formula for CI calculation was used:

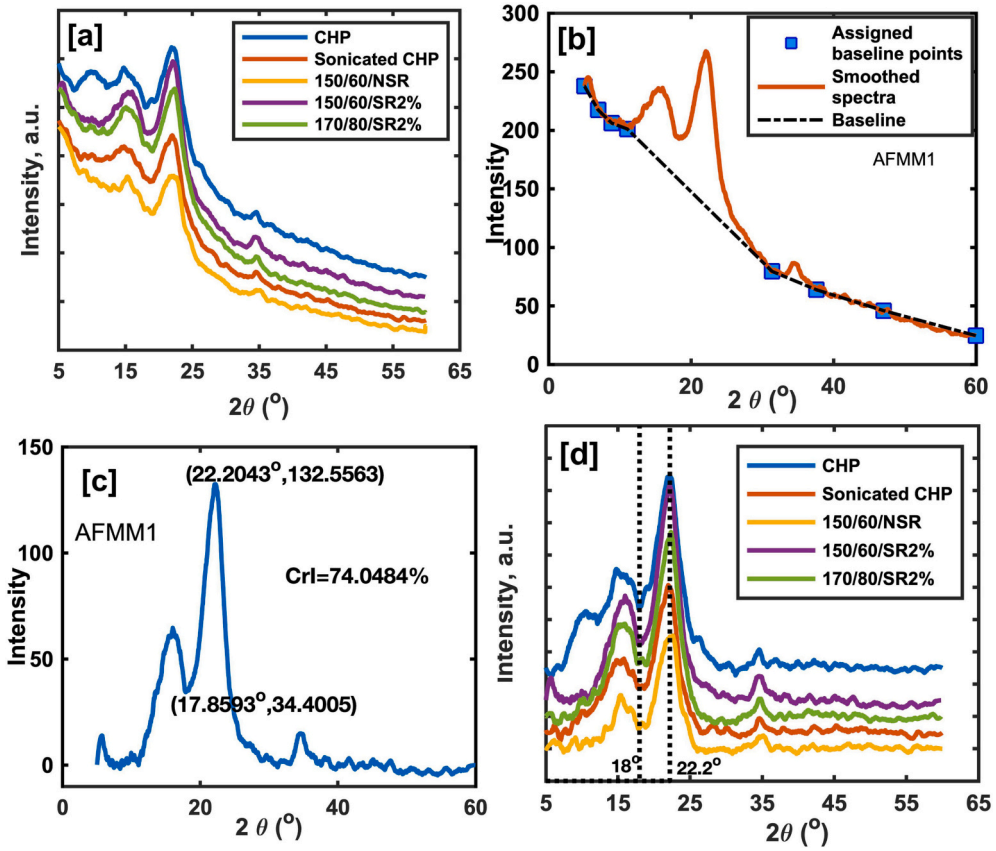

Fig. 3. XRD analysis curves. (a) Smoothed diffractograms of all samples, (b) Smoothed diffractogram and linear baseline of raw CHP, (c) baseline-corrected diffractogram of raw CHP, and (d) baseline-corrected diffractograms of all samples.

Table 3
DAEM kinetic parameters of each stage.

Sample	Stage I	Stage II	Stage III
Raw CHP	$A = 3.2580 \times 10^{12}$	$A = 59.5211 \times 10^{12}$	$A = 10.6380 \times 10^{12}$
	$E_0 = 149.9880$	$E_0 = 179.6435$	$E_0 = 213.6235$
	$\sigma = 3.5999$	$\sigma = 3.1530$	$\sigma = 19.3228$
	$R^2 = 0.9947$	$R^2 = 0.9968$	$R^2 = 0.9910$
	FQ = 3.33 %	FQ = 2.63 %	FQ = 4.21 %
Sonicated CHP	$A = 0.9605 \times 10^{12}$	$A = 22.2085 \times 10^{12}$	$A = 30.6391 \times 10^{12}$
	$E_0 = 147.2310$	$E_0 = 180.0872$	$E_0 = 222.3320$
	$\sigma = 3.8606$	$\sigma = 3.4653$	$\sigma = 19.3228$
	$R^2 = 0.9965$	$R^2 = 0.9985$	$R^2 = 0.9950$
	FQ = 3.03 %	FQ = 1.83 %	FQ = 3.60 %
150/60/NSR	$A = 4.1012 \times 10^{12}$	$A = 20.0632 \times 10^{12}$	$A = 6.9568 \times 10^{12}$
	$E_0 = 154.5528$	$E_0 = 179.9809$	$E_0 = 218.3786$
	$\sigma = 3.0432$	$\sigma = 3.5101$	$\sigma = 20.4627$
	$R^2 = 0.9981$	$R^2 = 0.9989$	$R^2 = 0.9966$
	FQ = 2.35 %	FQ = 1.56 %	FQ = 2.91 %
150/60/SR2%	$A = 2.6562 \times 10^{12}$	$A = 7.3668 \times 10^{12}$	$A = 64.5462 \times 10^{12}$
	$E_0 = 153.6176$	$E_0 = 178.0808$	$E_0 = 236.3405$
	$\sigma = 3.0360$	$\sigma = 5.4716$	$\sigma = 18.9854$
	$R^2 = 0.9971$	$R^2 = 0.9972$	$R^2 = 0.9977$
	FQ = 2.91 %	FQ = 2.42 %	FQ = 2.1964 %
170/80/SR2%	$A = 2.6917 \times 10^{12}$	$A = 7.7375 \times 10^{12}$	$A = 191.0652 \times 10^{12}$
	$E_0 = 153.3228$	$E_0 = 179.4018$	$E_0 = 238.3159$
	$\sigma = 3.0913$	$\sigma = 5.1158$	$\sigma = 20.7592$
	$R^2 = 0.9984$	$R^2 = 0.9984$	$R^2 = 0.9958$
	FQ = 2.18 %	FQ = 1.85 %	FQ = 3.03 %

$$CI\ (\%) = \frac{(I_{002} - I_{am})}{I_{002}} \times 100 \quad (26)$$

where I_{002} is the maximum intensity of 002 diffraction plane and I_{am} is the minimum height between peak 002 and 101 denoting amorphous scattering. As the XRD spectra generally appear with crowded noise the signals are usually smoothed. In this work, the smooth function of Matlab® (version 2021b) with Savitzky-Golay method was used.

3. Results and discussion

This work explored the application of DAEM employing thermogravimetry kinetics to 5 samples to obtain their lignocellulose compositions. The samples were raw CHP, sonicated CHP, and 3 subcritical water-treated CHP samples. All subcritical water-treated samples were sonicated first prior to the treatment. Sample code 150/60/NSR represented subcritical treatment at 150 °C, 60 min with surfactant (sodium dodecyl sulfate) addition. Sample code 150/60/SR2% represented subcritical treatment at 150 °C, 60 min, and 2 % surfactant addition while 170/80/SR2% stood for subcritical treatment at 170 °C, 80 min, and 2 % surfactant addition.

3.1. Material proximate and ultimate characteristics

Proximate and ultimate analyses provide knowledge of biomass characteristics based on the compounds, elements, and energy content of biomass. Table 1 presented the results of proximate and ultimate analysis, as well as the gross caloric value of raw CHP in this study. The moisture content was as low as that of several residual agroindustrial biomass reported by (Cavalaglio et al., 2020), which were in the range of 6–8.5 %. Low moisture characteristic (<10 %) of biomass is desirable as

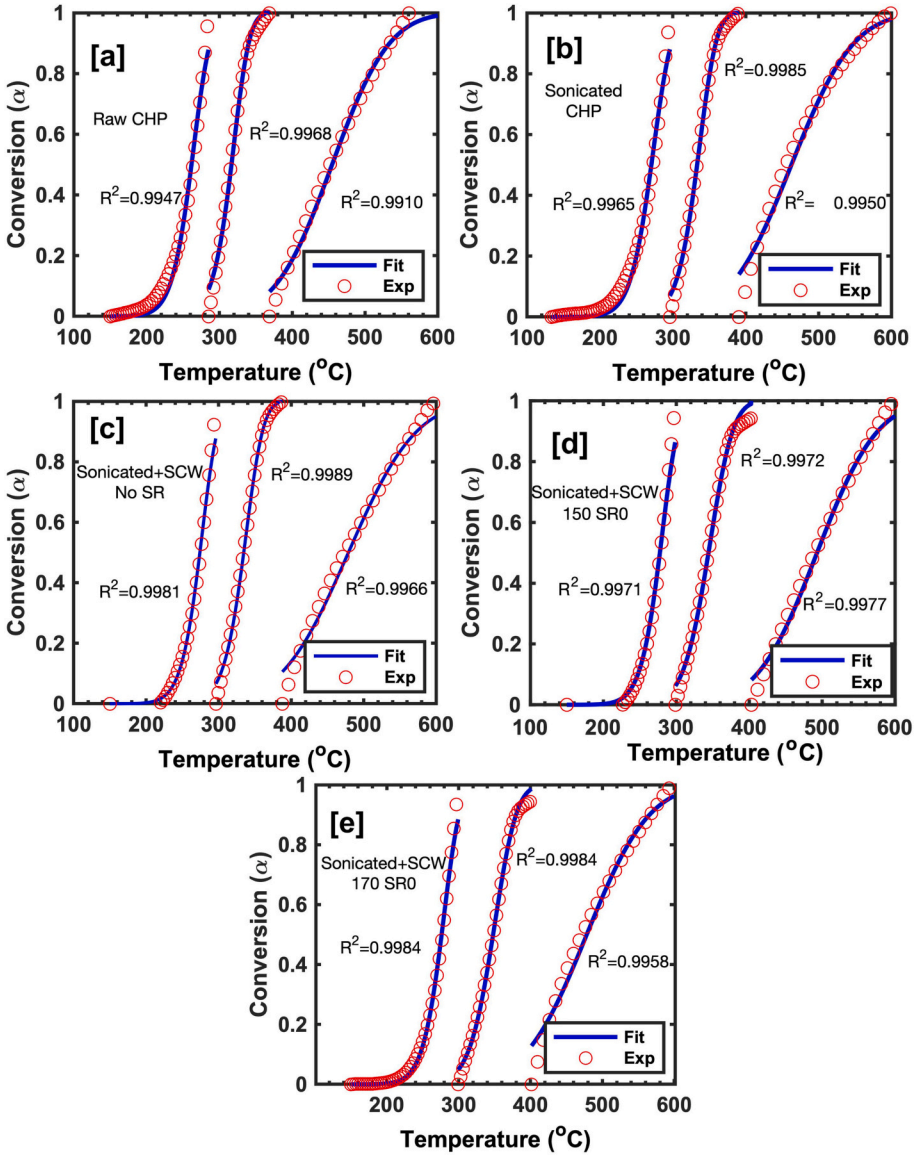

Fig. 4. The conversion profile in each of the pyrolysis stages. (a) Raw CHP, (b) sonicated CHP using water medium at 60 °C for 30 min, and sonicated and SCW treated at (c) 150 °C for 60 min without surfactant addition, (d) 150 °C for 60 min with 2 % surfactant addition, and (e) 170 °C for 80 min with 2 % surfactant addition.

it indicates the suitability for combustion and pyrolysis application (Gogoi et al., 2018; Santos et al., 2020). The highest content of CHP from the proximate test was the volatile matter. The second-highest component in the proximate analysis was fixed carbon. The volatile matter comprises condensable and no-condensable vapor released upon biomass heating while the fixed carbon represents the solid combustible residue after solid heating (Onokwai et al., 2022). The ash content was low (3.75 %) and the sulfur content was very low (0.07 %). It has been reported that the main constituents of ash include calcium, sodium, silicon, phosphorous, and magnesium. Woody biomass contained very low ash (<1 %). Among biomass, lignocellulose has the lowest ash content, which is <10 % (Leng et al., 2020).

The ultimate analysis results showed that the material has a high content of C and O elements. The content of element N was very low, probably because of the low protein content as reported by (Leng et al., 2020) that the biomass nitrogen content was positively related to its protein content. The caloric value represents the heat released upon combustion and approximates to high heating value (HHV) (Meyer et al., 2022).

The proximate and ultimate analyses of coconut husk from other work (Lopes and Tannous, 2020) were also shown in the table as a comparison. It was shown in Table 1 that the elemental and energy content of the raw CHP in this study were comparable with the presented other work. The analyses results revealed the potential of raw CHP as a thermal conversion feedstock.

3.2. *Thermogravimetric profiles*

Thermogravimetry analysis (TGA) performed at nonisothermal conditions was generally used to study the pyrolysis reaction kinetic as reactor design for biomass pyrolysis for alternative biofuel production gains much interest. A kinetic investigation based on the multistep reaction mechanism of lignocellulose had been performed by several investigators (Chen et al., 2015; Kim et al., 2022; Lopes and Tannous, 2020). Due to biomass complexity and pyrolysis products, another model-fitting approach involving three-parallel decomposition reactions of main components (hemicellulose, cellulose, and lignin) using DAEM was proposed for thermogravimetry (TG) kinetic elaboration. DAEM is

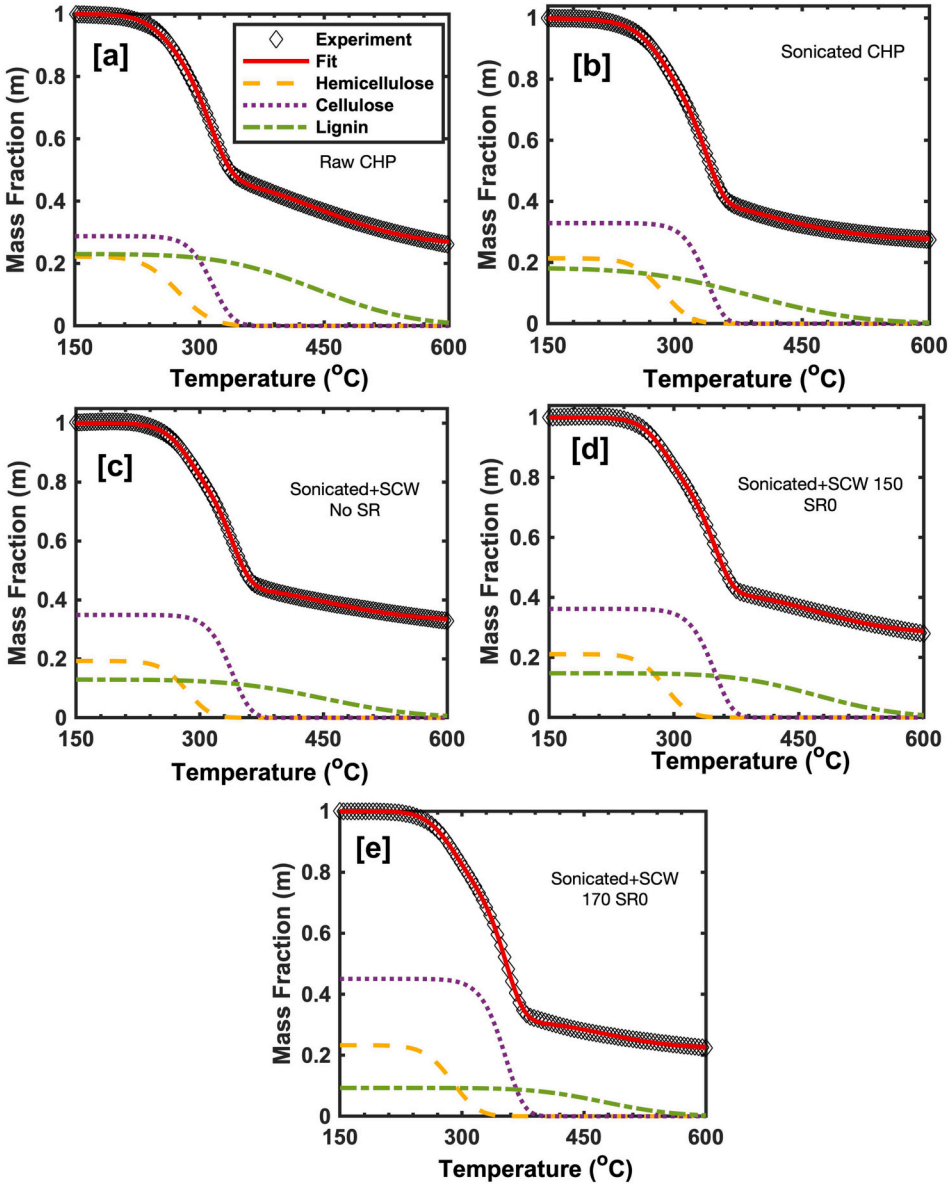

Fig. 5. The total and lignocellulosic components mass fraction. (a) Raw CHP, (b) sonicated CHP using water medium at 60 °C for 30 min, and sonicated and SCW treated at (c) 150 °C for 60 min without surfactant addition, (d) 150 °C for 60 min with 2 % surfactant addition, and (e) 170 °C for 80 min with 2 % surfactant addition.

very accurate in representing the devolatilization kinetic of biomass (Arenas et al., 2019). In a such kinetic analysis of biomass, the compositions of its three main components were simultaneously evaluated.

The general profile of the biomass thermogram (TG curve) depicted the remaining weight of volatile substances as a function of temperature as shown in Fig. 1a for raw CHP. The weight loss resulted from the numerous reactions in each of the three main component (hemicellulose, cellulose, and lignin) decompositions. The devolatilization or decomposition of the biomass started after all the moisture content evaporates upon heating. The total reaction conversion profile (obtained using Eq. (4), in Subsection 2.4.1) for raw CHP was shown in Fig. 1b. It has been reported that there were decomposition zones appearing in the weight loss (TG) curve. Hemicellulose decomposed at 220–315 °C (Dhyani and Bhaskar, 2018; Hu et al., 2016). Cellulose decomposed at 315–400 °C (Dhyani and Bhaskar, 2018). Lignin had the slowest decomposition rate among the others and a wider decomposition temperature at 160–900 °C (Hu et al., 2016; Huang et al., 2011). However, those three reaction regions tend to overlap and the weight loss curve or TG curve does not sharply separate into the decomposition zones (Cheng et al., 2015).

DTG and DDTG curves can be employed to obtain biomass decomposition zones (Chen et al., 2015). Hemicellulose and cellulose decomposed independently of one another and hemicellulose was the first component that devolatilizes. This was shown by the increase of the DTG curve until a shoulder was reached. The following peak showed the highest cellulose decomposition rate. This first shoulder of the DTG curve was marked by the attainment of the first minimum point of the DDTG curve. Lignin decomposed slowly over a very broad temperature range and the peak of this decomposition was attained at the lowest rate of cellulose decomposition. This was represented by the second shoulder of the DDTG curve. The construction of DDTG curve for each of the samples enabled the estimation of temperature ranges at which hemicellulose, cellulose, and lignin decomposed.

Table 4
Three parallel DAEM kinetic parameter and lignocellulosic composition.

Sample	Hemicellulose	Cellulose	Lignin	R^2 (F) (FQ)
Raw CHP	$A = 1.5582 \times 10^{12}$	$A = 5.0000 \times 10^{13}$	$A = 1.16831 \times 10^{13}$	1.00
	$E_0 = 150.4862$	$E_0 = 177.9628$	$E_0 = 210.6992$	(0.0033)
	$\sigma = 7.4959$	$\sigma = 3.7456$	$\sigma = 26.4131$	(0.34 %)
	$c_H = 0.3000$	$c_C = 0.3886$	$c_L = 0.3496$	
	%wt = 30	%wt = 38.86	%wt = 34.96	
Sonicated CHP	$A = 1.2020 \times 10^{11}$	$A = 2.31081 \times 10^{13}$	$A = 3.41834 \times 10^{13}$	1.00
	$E_0 = 141.8962$	$E_0 = 180.4165$	$E_0 = 200.8217$	(7.837e-04)
	$\sigma = 4.8349$	$\sigma = 1.75935$	$\sigma = 30.0196$	(0.17 %)
	$c_H = 0.2949$	$c_C = 0.4538$	$c_L = 0.2513$	
	%wt = 29.49	%wt = 45.38	%wt = 25.13	
150/60/NSR	$A = 5.3581 \times 10^{12}$	$A = 2.06195 \times 10^{13}$	$A = 1.18691 \times 10^{13}$	1.00
	$E_0 = 159.3543$	$E_0 = 180.7184$	$E_0 = 210.2218$	(0.0026)
	$\sigma = 5.0594$	$\sigma = 2.1344$	$\sigma = 27.554$	(0.30 %)
	$c_H = 0.31$	$c_L = 0.\ 4800$	$c = 0.2100$	
	%wt = 31	%wt = 48	%wt = 21	
150/60/SR2%	$A = 1.0 \times 10^{13}$	$A = 2.8477 \times 10^{12}$	$A = 5.0000 \times 10^{13}$	1.00
	$E_0 = 162.9191$	$E_0 = 173.1915$	$E_0 = 228.0802$	(0.0016)
	$\sigma = 5.0252$	$\sigma = 2.0084$	$\sigma = 23.6944$	(0.24 %)
	$c_H = 0.2929$	$c_C = 0.5025$	$c_L = 0.2046$	
	%wt = 29.29	%wt = 50.25	%wt = 20.46	
170/80/SR2%	$A = 1.3822 \times 10^{12}$	$A = 7.6521 \times 10^{12}$	$A = 5.000 \times 10^{13}$	1.00
	$E_0 = 153.6578$	$E_0 = 179.7031$	$E_0 = 229.2353$	(0.0023)
	$\sigma = 5.1768$	$\sigma = 2.6232$	$\sigma = 19.9721$	(0.28 %)
	$c_H = 0.300$	$c_C = 0.5804$	$c_L = 0.1196$	
	%wt = 30	%wt = 58.04	%wt = 11.96	

3.3. Raw and pretreated CHP thermogravimetric stage

The TG, DTG, and DDTG curves of raw and treated CHP of this work were shown in Fig. 2a–e. The shape of the curves exactly followed the pattern shown in Fig. 1a. In each of the figures (Fig. 2a–e), the normalized remaining mass fraction (m) was constant up to above 200 °C at which it started to decline very rapidly. From Fig. 2, the stages of decomposition can be identified and presented in Table 2. The initial temperatures of each stage (T_i) were displayed in that table.

As shown in Table 2, all samples, raw and pretreated CHP, started the first stage at 150 °C where the water vaporization had stopped. At this temperature, the DTG and DDTG values were zero. The temperature where a shoulder existed on the DTG curve and marked the end of stage I (hemicellulose decomposition) was found at 285–300 °C. This agreed with other works reporting at 250–300 °C (Hu et al., 2016). The third stage started at around 368.83–401.33 °C. These stage temperature ranges assignment were used for obtaining the stage kinetic parameters (A_i, $E_{0,i}$, and σ_i).

The peak temperatures of DTG curves (T_{peak}) were in the range of 319–357 °C. It is similar to other lignocellulose materials. Chen et al. (2015) reported T_{peak} in the range of 321.79–350 °C for pinewood sawdust, fern, wheat stalk, sugarcane bagasse, and jute. Hu et al. (2016) also revealed the peak temperature to be in a similar range (300–350 °C). Kim et al. (2022) reported DTG peak at 361–385 °C for Hinoki cypress, pinewood, birchwood, and wood pellets. As shown in Table 2, the pretreatment (sonication and subcritical waer) shifted the peak to higher temperatures. This implied that the pretreated CHP become more thermally stable. According to Jiang et al. (2019), less crystalline material would show less endothermic activity and decompose more rapidly upon heating. Another work by (Hideno, 2020) reported that alkaline-peroxide biomass treatment caused increases in thermal decomposition temperature as their cellulose content increased while their hemicellulose and lignin decreased.

In order to relate the peak temperature shifting with sample crystallinity, the crystallinity index values of the samples were evaluated from the XRD spectra by using Eq. (26). The XRD spectra of the samples after being smoothed using the Savitzky-Golay method as explained in Subsection 2.5 were shown in Fig. 3a. In Fig. 3b, the baseline correction process of subcritical water pretreated CHP sample (150/60/SR2%) was exemplified. Some manually chosen baseline points were visualized as star bullets. Two adjacent points were connected with linear lines and hence linear functions were used to represent the baselines between two adjacent chosen points. After subtracting the baseline values from the corresponding intensity, the diffractogram shape shown in Fig. 3b changed as shown in Fig. 3c. On that figure, the I_{002} and I_{am} used for the CI evaluation, appearing at 2 theta angles of 22.2043°, and 17.8593°, were 132.5563, and 34.4005, respectively. This resulted in a CI value of 74.0484 %. The I_{002} and I_{am} peaks for the treated CHP samples in Fig. 3d were relatively similar to those of raw CHP, which were in the vicinity of 22°, and 18°, respectively. The CI values for all of the samples were also shown in Table 2. The treatment of CHP increased crystallinity as it increased the cellulose compositions of the treated samples. The highest CI, which was 82.7632 %, resulted from subcritical water-treated CHP at 150 °C and 60 min with no surfactant addition. However, surfactant addition in subcritical water treatment reduced crystallinity from 82.7632 to 74.0484 %. The increasing severity attempted by increasing temperature (from 150 to 170 °C) and time (from 60 to 80 min) for subcritical water treatment further reduced CI slightly to 72.1946 %. The increasingly severe condition may affect the destruction of the material internal crystalline structure by providing energy to break hydrogen bonds as the H-bond is one of the physical interactions that stabilize the cellulose microfibril (Sarker et al., 2021; Shen and Gnanakaran, 2009). The results of crystallinity index showed that they did not directly correlate with the peak temperature shifting in this work.

3.4. Three stage and pseudocomponent kinetic parameters

The identified stage temperature ranges were used for the determination of non-isothermal kinetic parameters of the single reaction occurring in each stage. Those parameters were a pre-exponential factor, mean, and standard deviation activation energy (A, E_0, and σ). This required that the stage initial and final temperatures, shown in Table 2, be applied for the iterative calculations according to Eq. (14). For each of the stages, initial guess values of A, E_0, and σ were chosen based on the results of other works for different systems. Cai et al. (2013) investigated the DAEM adopting pyrolysis kinetics of xylan, cellulose, and several biomass. The preexponential factors (1/s) were 5.0350×10^{12} for xylan, 8.0168×10^{13} for cellulose, as well as $0.50119–1.2552 \times 10^{13}$, $4.1495–8.892 \times 10^{13}$, and $0.10139–3.4356 \times 10^{16}$ for the first, second, and third pseudocomponent of the biomass, respectively. The mean activation energy values (kJ/mol) were 178.311 ± 2.127 for xylan, 210.037 ± 2.924 for cellulose, as well as 169.710–186.776, 199.966–207.381, and 236.344–271.758 for the first, second, and third pseudocomponent of the biomass, respectively. The standard deviation activation energy values (kJ/mol) were 5.848 ± 0.063 for xylan, 0.944 ± 0.013 for cellulose, as well as 5.375–5.888, 1.126–1.339, and 26.583–41.767 for the first, second, and third pseudocomponent of the biomass, respectively. In this work, upon the introduction of initial guess values, then iterative computations were carried out subject to the fulfillment of the objective function of Eq. (15) to obtain the kinetic parameters for each stage. For each of those 3 stages, the calculation involved 200–300 data within the stage temperature range. The results shown in Table 3 were comparable to the work of Chen et al. (2015). The model-fitting results were also very good as seen in Table 3 that the R^2 values of higher than 0.99 and the fit quality (FQ) values of <4.5 %. It suggested that DAEM had satisfyingly approached the decomposition reaction. This is reflected in the conversion profile of each stage in Fig. 4a–d. Although relatively large deviations of the calculated conversion from experimental values appeared at low conversion for stage I

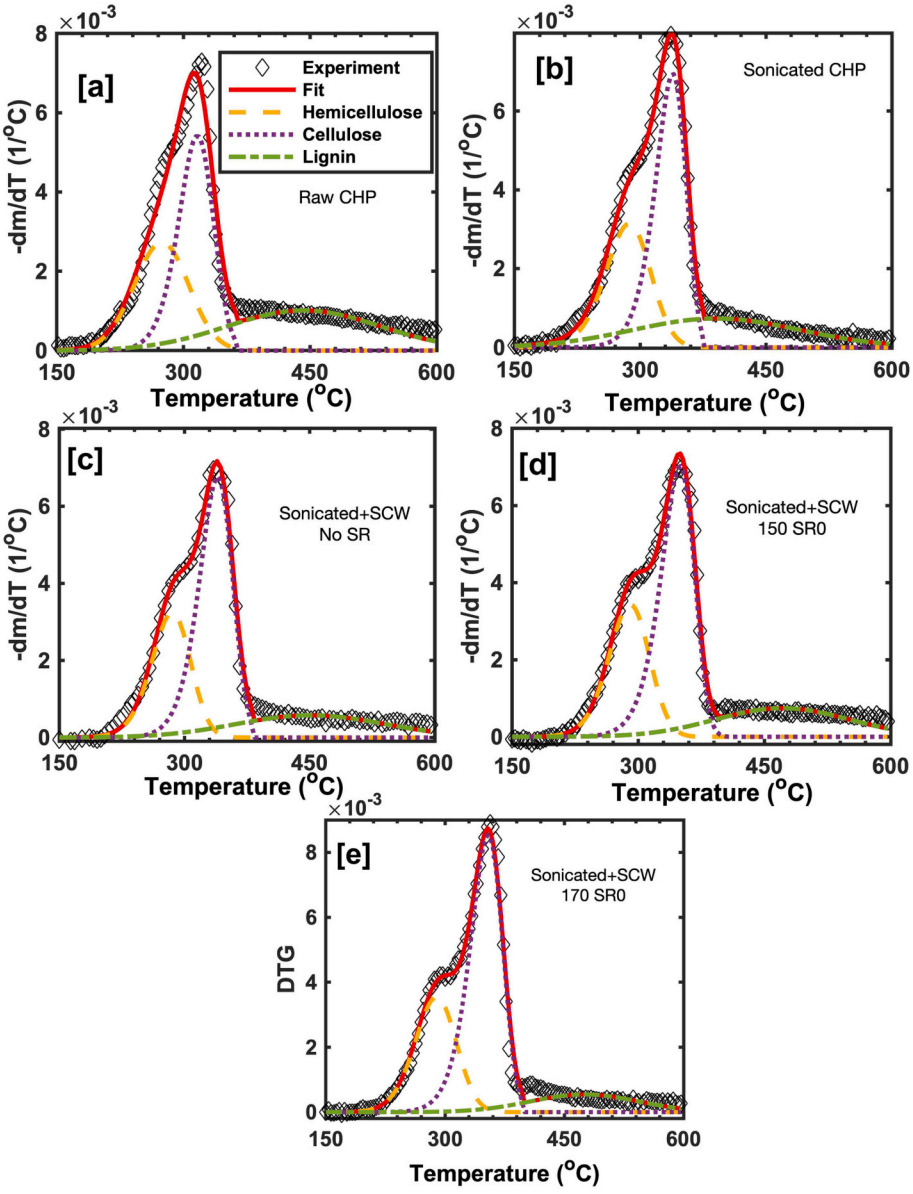

Fig. 6. The total and lignocellulosic component DTG profile. (a) Raw CHP, (b) sonicated CHP using water medium at 60 °C for 30 min, and sonicated and SCW treated at (c) 150 °C for 60 min without surfactant addition, (d) 150 °C for 60 min with 2 % surfactant addition, and (e) 170 °C for 80 min with 2 % surfactant addition.

or at high conversion for stage II and III, the DAEM assuming kinetic model estimated the conversion very closely at the rest of the data.

Fig. 5 illustrated the fractional total mass loss curves of the investigated samples, both from the experimental, and computed (fit) data. The graphs in that figure also depicted the three pseudocomponent mass losses. The fitted fractional total and component mass loss curves were the results of iterative computation of Eq. (20). The accomplishment of the computations acquired the introduction of initial guess values for 11 parameters to be determined. Nine of the 11 parameters were kinetic parameters of the three pseudocomponents, where each of those components had 3 kinetic parameters (A_i, $E_{0,i}$, and σ_i). The rest 2 parameters were the compositions of hemicellulose and cellulose. The lignin composition was obtained using the unity composition summation rule requirement. Similar to the iterative computation process of the aforementioned 3-stage kinetic parameters, this 11-parameter calculation also needed an establishment of initial guess values. This was done using 9 values of previously obtained stage kinetic parameters. Meanwhile, 2 initial guess values for pseudocomponent composition were given based on the general elsewhere published data of lignocellulose composition.

Table 4 presented the results for decomposition kinetic parameters as well as the composition for hemicellulose, cellulose, and lignin. The mean activation energy (E_0) was 141–163, 173–181, and 200–230 kJ/mol for hemicellulose, cellulose, and lignin, respectively. The standard deviation activation energy (σ) was 4.8–7.5, 1.76–3.75, and 19–28 kJ/mol for hemicellulose, cellulose, and lignin respectively. The pre-exponential factor (A) values ranged from 1.20×10^{11} to 5.00×10^{13} s^{-1}. The work of Kim et al. (2022) also employed a multi-step kinetic model but did not use DAEM and showed that lignin has the lowest activation energy (27.4–35.2 kJ/mol) followed by hemicellulose (109–117 kJ/mol) and cellulose (193–232 kJ/mol), respectively. This trend was similar to the work of Lopes and Tannous (2020). Kristanto et al. (2021) reported the value of E_0 and σ for commercial cellulose which were 178.6488 and 1.6320 kJ/mol, respectively by using Gaussian distribution function for DAEM. The value of E_0 was similar to that in this work. From Table 4 it can also be seen that the mean activation energy value trend for all samples are $E_{0,lignin} > E_{0,cellulose} > E_{0,}$

hemicellulose. The activation energy represents the reaction obstacle that should be overcome for a reaction to occur. The highest value of mean activation energy of lignin revealed that lignin was the most thermally stable component of these raw and treated CHP. According to the table, the activation energy standard deviation trend was $\sigma_{\text{lignin}} > \sigma_{\text{cellulose}} > \sigma_{\text{hemicellulose}}$. This trend results agreed with the other work by (Chen et al., 2015; Hu et al., 2016). The highest standard deviation activation energy attribution of lignin among the other two components showed that lignin had the widest range of activation energy. Those trends of activation energy and its standard deviation imparted the slowest decomposition reaction rate and the widest reaction temperature range to the lignin component of the investigated raw and treated CHP. There was no trend for the pre-exponential values in this work and this agreed with Chen et al. (2015). By using a different procedure, three independent parallel schemes for raw coconut fiber thermogravimetry kinetics had also been studied by (Lopes and Tannous, 2020), who applied DTG deconvolution procedure without incorporating DAEM and used an 8th-degree rational function approximation instead of that shown in Eq. (7). The conversions of volatile substances were fitted using a first-order reaction model for hemicellulose and cellulose, while a second-order reaction model for lignin at 3 different heating rates (5, 10, and 15 °C/min) in that work. The lignocellulose compositions obtained were exactly the same for those 3 heating rates, and surprisingly the values were very close to those obtained in this work here (shown in Table 4) which were 0.3, 0.4, and 0.35 for hemicellulose, cellulose, and lignin, respectively despite its larger fit quality (2.8–3 %).

The DTG curves implying the decomposition rate in Fig. 6a–d exhibited that the model fit approximated the experiment data very well for all the samples. The fit DTG curves were obtained by numerically computing the first derivatives of the lignocellulose biomass mass changes obtained in Eq. (20). The shoulder part of the DTG curves was clearly observed on the model fit curves (Fig. 6b–d) except for the raw CHP (Fig. 6a). The inexistence of the shoulder on the model fit curve of Fig. 6a indicated sharper overlap between the hemicellulose and cellulose. This caused the end deconvolution peak curves of hemicellulose closely approach that of cellulose. Since the mass changes data can be obtained from the model for each of the three components (hemicellulose, cellulose, and lignin) and depicted in Fig. 5, the component DTG curves can also be constructed and shown in Fig. 6 as the deconvolution peak curves of the corresponding biomass model fit DTG curves. These were done by numerically computing the first derivatives of mass changes data of hemicellulose, cellulose, and lignin. The DTG curves of the three components in Fig. 6 showed the peak temperatures of hemicellulose, cellulose, and lignin in the vicinity of 270–290, 314–354, and 390–480 °C, respectively. The deconvolution peak curves of lignin described slow rate lignin decomposition which occurred at a wide range of temperatures (160–600 °C).

4. Conclusions

The TGA pyrolysis kinetics employing DAEM has been favorably applied to determine the raw and pretreated coconut husk powder composition. The stage simulation results are very satisfying, with R^2 >0.99 and the fit quality <4.5 %. The fractional mass losses are excellently simulated with R^2 attaining 1 and the fit quality <0.5 %. The raw and pretreated CHP compositions (%wt) for hemicellulose, cellulose, and lignin are 29–31, 38–58, and 11–35, respectively. The raw CHP composition obtained agrees with the other work. The developed method can be used as an alternative for time-saving lignocellulose compositional analysis for industrial purposes.

CRediT authorship contribution statement

Akbarningrum Fatmawati: Conceptualization, Investigation, Writing. **Tantular Nurtono:** Review, Supervision. **Arief Widjaja:** Review, Supervision.

Funding

This work was supported by Lembaga Pengelola Dana Pendidikan (LPDP), Government of Indonesia (GOI) organizing agency of endowment fund for education, [grant no. 201908210215431, year 2019].

Declaration of competing interest

The authors declare that they have no known competing financial interests or personal relationships that could have appeared to influence the work reported in this paper.

Data availability

Data will be made available on request.

Acknowledgement

The authors acknowledged the support of several colleagues including Saiyyidah Tus Zuhroh, Jessica Aalya Kaammiliaa, Laksmi Cahyaningati Puteri for the technical assistance of the sample preparation, and Stanley Abel Hartanto for the article artwork improvement.

References

Aghili, A., 2021. Representation and evaluation of the Arrhenius and general temperature integrals by special functions. Thermochim. Acta 705, 179034. https://doi.org/10.1016/J.TCA.2021.179034.

Arenas, C.N., Navarro, M.V., Martínez, J.D., 2019. Pyrolysis kinetics of biomass wastes using isoconversional methods and the distributed activation energy model. Bioresour. Technol. 288, 121485 https://doi.org/10.1016/J.BIORTECH.2019.121485.

Baruah, J., Nath, B.K., Sharma, R., Kumar, S., Deka, R.C., Baruah, D.C., Kalita, E., 2018. Recent trends in the pretreatment of lignocellulosic biomass for value-added products. Front Energy Res 6, 141. https://doi.org/10.3389/FENRG.2018.00141/BIBTEX.

Cai, J., Wu, W., Liu, R., Huber, G.W., 2013. A distributed activation energy model for the pyrolysis of lignocellulosic biomass. Green Chem. 15, 1331–1340. https://doi.org/10.1039/C3GC36958G.

Cai, J., He, Y., Yu, X., Banks, S.W., Yang, Y., Zhang, X., Yu, Y., Liu, R., Bridgwater, A.V., 2017. Review of physicochemical properties and analytical characterization of lignocellulosic biomass. Renew. Sust. Energ. Rev. 76, 309–322. https://doi.org/10.1016/J.RSER.2017.03.072.

Cavalaglio, G., Cotana, F., Nicolini, A., Coccia, V., Petrozzi, A., Formica, A., Bertini, A., 2020. Characterization of Various Biomass Feedstock Suitable for Small-Scale Energy Plants as Preliminary Activity of Biocheaper Project. Sustainability 2020, Vol. 12, Page 6678 12, 6678. doi:https://doi.org/10.3390/SU12166678.

Chen, Z., Hu, M., Zhu, X., Guo, D., Liu, S., Hu, Z., Xiao, B., Wang, J., Laghari, M., 2015. Characteristics and kinetic study on pyrolysis of five lignocellulosic biomass via thermogravimetric analysis. Bioresour. Technol. 192, 441–450. https://doi.org/10.1016/J.BIORTECH.2015.05.062.

Cheng, Z., Wu, W., Ji, P., Zhou, X., Liu, R., Cai, J., 2015. Applicability of Fraser-Suzuki function in kinetic analysis of DAEM processes and lignocellulosic biomass pyrolysis processes. J. Therm. Anal. Calorim. 119, 1429–1438. https://doi.org/10.1007/S10973-014-4215-3/METRICS.

Cheng, F., Sun, J., Wang, Z., Zhao, X., Hu, Y., 2019. Organosolv fractionation and simultaneous conversion of lignocellulosic biomass in aqueous 1,4-butanediol/acidic ionic-liquids solution. Ind. Crop. Prod. 138, 111573 https://doi.org/10.1016/J.INDCROP.2019.111573.

Dash, S., Thakur, S., Bhavanam, A., Gera, P., 2022. Catalytic pyrolysis of alkaline lignin: a systematic kinetic study. Bioresour Technol Rep 18, 101064. https://doi.org/10.1016/J.BITEB.2022.101064.

Deng, C., Cai, J., Liu, R., 2009. Kinetic analysis of solid-state reactions: evaluation of approximations to temperature integral and their applications. Solid State Sci. 11, 1375–1379. https://doi.org/10.1016/J.SOLIDSTATESCIENCES.2009.04.009.

Dhyani, V., Bhaskar, T., 2018. A comprehensive review on the pyrolysis of lignocellulosic biomass. Renew. Energy 129, 695–716. https://doi.org/10.1016/J.RENENE.2017.04.035.

Emiola-Sadiq, T., Zhang, L., Dalai, A.K., 2021. Thermal and kinetic studies on biomass degradation via thermogravimetric analysis: a combination of model-fitting and model-free approach. ACS Omega 6, 22233–22247. https://doi.org/10.1021/ACSOMEGA.1C02937/ASSET/IMAGES/LARGE/AO1C02937_0008.JPEG.

Gogoi, M., Konwar, K., Bhuyan, N., Borah, R.C., Kalita, A.C., Nath, H.P., Saikia, N., 2018. Assessments of pyrolysis kinetics and mechanisms of biomass residues using thermogravimetry. Bioresour Technol Rep 4, 40–49. https://doi.org/10.1016/J.BITEB.2018.08.016.

Hideno, A., 2020. Thermogravimetric analysis-based characterization of suitable biomass for alkaline peroxide treatment to obtain cellulose and fermentable sugars. Bioresources 15, 6217–6229. https://doi.org/10.15376/biores.15.3.6217-6229.
Hodgson, D., Bains, P., Moorhouse, J., 2022. Bioenergy – Analysis - IEA [WWW Document]. URL https://www.iea.org/reports/bioenergy (accessed 12.4.22).
Hu, M., Chen, Z., Wang, S., Guo, D., Ma, C., Zhou, Y., Chen, J., Laghari, M., Fazal, S., Xiao, B., Zhang, B., Ma, S., 2016. Thermogravimetric kinetics of lignocellulosic biomass slow pyrolysis using distributed activation energy model, Fraser–Suzuki deconvolution, and iso-conversional method. Energy Convers. Manag. 118, 1–11. doi:https://doi.org/10.1016/J.ENCONMAN.2016.03.058.
Huang, Y.F., Kuan, W.H., Chiueh, P.T., Lo, S.L., 2011. A sequential method to analyze the kinetics of biomass pyrolysis. Bioresour. Technol. 102, 9241–9246. https://doi.org/10.1016/J.BIORTECH.2011.07.015.
IEA, 2021. CO2 emissions – Global Energy Review 2021 – Analysis - IEA [WWW Document]. URL https://www.iea.org/reports/global-energy-review-2021/co2-emissions (accessed 12.4.22).
Jiang, L. Qun, Wu, Y. Xiang, Wang, X. Bo, Zheng, A. Qing, Zhao, Z. Li, Li, H. Bin, Feng, X. Jun, 2019. Crude glycerol pretreatment for selective saccharification of lignocellulose via fast pyrolysis and enzyme hydrolysis. Energy Convers. Manag. 199, 111894 https://doi.org/10.1016/J.ENCONMAN.2019.111894.
Kim, H., Yu, S., Kim, M., Ryu, C., 2022. Progressive deconvolution of biomass thermogram to derive lignocellulosic composition and pyrolysis kinetics for parallel reaction model. Energy 254, 124446. https://doi.org/10.1016/J.ENERGY.2022.124446.
Kristanto, J., Azis, M.M., Purwono, S., 2021. Multi-distribution activation energy model on slow pyrolysis of cellulose and lignin in TGA/DSC. Heliyon 7. https://doi.org/10.1016/j.heliyon.2021.e07669.
Kuna, E., Behling, R., Valange, S., Chatel, G., Colmenares, J.C., 2017. Sonocatalysis: a potential sustainable pathway for the valorization of lignocellulosic biomass and derivatives. Top. Curr. Chem. 375, 1–20. https://doi.org/10.1007/S41061-017-0122-Y/TABLES/1.
Leng, L., Yang, L., Chen, J., Leng, S., Li, Hailong, Li, Hui, Yuan, X., Zhou, W., Huang, H., 2020. A review on pyrolysis of protein-rich biomass: nitrogen transformation. Bioresour. Technol. 315, 123801 https://doi.org/10.1016/J.BIORTECH.2020.123801.
Ling, Z., Chen, S., Zhang, X., Xu, F., 2017. Exploring crystalline-structural variations of cellulose during alkaline pretreatment for enhanced enzymatic hydrolysis. Bioresour. Technol. 224, 611–617. https://doi.org/10.1016/J.BIORTECH.2016.10.064.
Lopes, F.C.R., Tannous, K., 2020. Coconut fiber pyrolysis decomposition kinetics applying single- and multi-step reaction models. Thermochim. Acta 691, 178714. https://doi.org/10.1016/J.TCA.2020.178714.
Menon, V., Rao, M., 2012. Trends in bioconversion of lignocellulose: biofuels, platform chemicals & biorefinery concept. Prog. Energy Combust. Sci. 38, 522–550. https://doi.org/10.1016/J.PECS.2012.02.002.
Meyer, J.A., Strydom, C.A., Bunt, J.R., Uwaoma, R.C., 2022. Pyrolysis products derived from co-processing of coal fines and microalgae. Bioresour Technol Rep 19, 101128. https://doi.org/10.1016/J.BITEB.2022.101128.
Nurika, I., Shabrina, E.N., Azizah, N., Suhartini, S., Bugg, T.D.H., Barker, G.C., 2022. Application of ligninolytic bacteria to the enhancement of lignocellulose breakdown and methane production from oil palm empty fruit bunches (OPEFB). Bioresour Technol Rep 17, 100951. https://doi.org/10.1016/J.BITEB.2022.100951.
Onokwai, A.O., Ajisegiri, E.S.A., Okokpujie, I.P., Ibikunle, R.A., Oki, M., Dirisu, J.O., 2022. Characterization of lignocellulose biomass based on proximate, ultimate, structural composition, and thermal analysis. Mater Today Proc 65, 2156–2162. https://doi.org/10.1016/J.MATPR.2022.05.313.
Prado, J.M., Lachos-Perez, D., Forster-Carneiro, T., Rostagno, M.A., 2016. Sub- and supercritical water hydrolysis of agricultural and food industry residues for the production of fermentable sugars: a review. Food Bioprod. Process. 98, 95–123. https://doi.org/10.1016/J.FBP.2015.11.004.
Raud, M., Kikas, T., Sippula, O., Shurpali, N.J., 2019. Potentials and challenges in lignocellulosic biofuel production technology. Renew. Sust. Energ. Rev. 111, 44–56. https://doi.org/10.1016/j.rser.2019.05.020.
Rego, F., Soares Dias, A.P., Casquilho, M., Rosa, F.C., Rodrigues, A., 2019. Fast determination of lignocellulosic composition of poplar biomass by thermogravimetry. Biomass Bioenergy 122, 375–380. https://doi.org/10.1016/J.BIOMBIOE.2019.01.037.
Ruiz, H.A., Rodríguez-Jasso, R.M., Fernandes, B.D., Vicente, A.A., Teixeira, J.A., 2013. Hydrothermal processing, as an alternative for upgrading agriculture residues and marine biomass according to the biorefinery concept: a review. Renew. Sust. Energ. Rev. 21, 35–51. https://doi.org/10.1016/J.RSER.2012.11.069.
Santos, V.O., Queiroz, L.S., Araujo, R.O., Ribeiro, F.C.P., Guimarães, M.N., da Costa, C.E. F., Chaar, J.S., de Souza, L.K.C., 2020. Pyrolysis of acai seed biomass: kinetics and thermodynamic parameters using thermogravimetric analysis. Bioresour Technol Rep 12, 100553. https://doi.org/10.1016/J.BITEB.2020.100553.
Sarker, T.R., Azargohar, R., Dalai, A.K., Meda, V., 2021. Enhancement of fuel and physicochemical properties of canola residues via microwave torrefaction. Energy Rep. 7, 6338–6353. https://doi.org/10.1016/J.EGYR.2021.09.068.
Shen, T., Gnanakaran, S., 2009. The stability of cellulose: a statistical perspective from a coarse-grained model of hydrogen-bond networks. Biophys. J. 96, 3032–3040. https://doi.org/10.1016/J.BPJ.2008.12.3953.
Sluiter, J.B., Ruiz, R.O., Scarlata, C.J., Sluiter, A.D., Templeton, D.W., 2010. Compositional analysis of lignocellulosic feedstocks. 1. Review and description of methods. J. Agric. Food Chem. 58, 9043–9053. https://doi.org/10.1021/JF1008023/SUPPL_FILE/JF1008023_SI_007.PDF.
Sluiter, A., Hames, B., Ruiz, R., Scarlata, C., Sluiter, J., Templeton, D., Crocker, D., 2012. Determination of Structural Carbohydrates and Lignin in Biomass [WWW Document]. Laboratory Analytical Procedure. https://www.nrel.gov/docs/gen/fy13/42618.pdf (accessed 12.5.22).
Sydney, E.B., Letti, L.A.J., Karp, S.G., Sydney, A.C.N., Vandenberghe, L.P. de S., de Carvalho, J.C., Woiciechowski, A.L., Medeiros, A.B.P., Soccol, V.T., Soccol, C.R., 2019. Current analysis and future perspective of reduction in worldwide greenhouse gases emissions by using first and second generation bioethanol in the transportation sector. Bioresour Technol Rep 7, 100234. https://doi.org/10.1016/J.BITEB.2019.100234.
Templeton, D.W., Wolfrum, E.J., Yen, J.H., Sharpless, K.E., 2016. Compositional analysis of biomass reference materials: results from an interlaboratory study. Bioenergy Res 9, 303–314. https://doi.org/10.1007/S12155-015-9675-1/FIGURES/3.
Van Geem, K., 2019. Kinetic modeling of the pyrolysis chemistry of fossil and alternative feedstocks. Computer Aided Chemical Engineering 45, 295–362. https://doi.org/10.1016/B978-0-444-64087-1.00006-1.
Vyazovkin, S., 2016. A time to search: finding the meaning of variable activation energy. Phys. Chem. Chem. Phys. 18, 18643–18656. https://doi.org/10.1039/C6CP02491B.
Xiang, A., Ebdon, J.R., Horrocks, A.R., Kandola, B.K., 2022. On the utility of thermogravimetric analysis for exploring the kinetics of thermal degradation of lignins. Bioresour Technol Rep 20, 101214. https://doi.org/10.1016/J.BITEB.2022.101214.